ELSEVIER

Conformation effect of oligosilane linker on photoinduced electron transfer of tetrasilane-linked zinc porphyrin–[60]fullerene dyads

Yuki Shibano [a], Mikio Sasaki [b], Hayato Tsuji [a,*], Yasuyuki Araki [b],
Osamu Ito [b,*], Kohei Tamao [a,c,*]

[a] *International Research Center for Elements Science (IRCELS), Institute for Chemical Research, Kyoto University, Uji, Kyoto 611-0011, Japan*
[b] *Institute of Multidisciplinary Research for Advanced Materials, Tohoku University, Katahira, Aoba-ku, Sendai 980-8577, Japan*
[c] *RIKEN Frontier Research System, 2-1 Hirosawa, Wako, Saitama 351-0198, Japan*

Abstract

A series of zinc porphyrin–[60]fullerene dyads linked by conformation-constrained tetrasilanes and permethylated tetrasilane have been synthesized for the evaluation of the conformation effect of the tetrasilane linkers on the photoinduced electron transfer. The excited-state dynamics of these dyads have been studied using the time-resolved fluorescence and absorption measurements. The fluorescence of the zinc porphyrin moiety in each dyad was quenched by the electron transfer to the fullerene moiety. The transient absorption measurements revealed that the final state of the excited-state process was a radical ion pair with a radical cation on the zinc porphyrin moiety and a radical anion on the fullerene moiety as a result of the charge separation. The charge separation and charge recombination rates were found to show only slight conformation dependence of the tetrasilane linkers, which is characteristic for the Si-linkages.
© 2006 Elsevier B.V. All rights reserved.

Keywords: Electron transfer; Porphyrin; Fullerene; Oligosilane; Conformation

1. Introduction

Electron transfer (ET) plays a key role in many essential biological reactions, such as in natural photosynthesis, in which an incident light causes a cascade of energy transfer (EN) and subsequent ET. Recently, various types of covalently linked donor–acceptor molecules have been synthesized for understanding and mimicking the ET and EN during the natural photosynthesis to develop an artificial photosynthesis as a new energy source [1]. The most widely investigated donor–acceptor systems are the porphyrin–fullerene hybrid molecules since the photoexcitation of these dyads induces a fast ET from the porphyrin to the fullerene moiety to generate long-lived charge-separated (CS) states [2,3] which are essential for the further transduction of the incident light energy [4]. Porphyrins are some of the most ideal donors and photo-sensitizers because of their low oxidation potentials as well as their expanded π-electron system which are suitable for efficient light-harvesting by covering the wide spectral range of the solar irradiation [5]. Fullerenes, such as C_{60}, have been revealed as promising photo-sensitizers and electron-acceptors due to the following unique structural and electronic properties [6–10]; the wide absorption range due to their extremely expanded π-electron systems, the low-lying LUMO, and the small reorganization energies which accelerate the forward ET process and decelerate the back ET process as described by the Marcus parabola [11].

Another important factor of the Marcus theory is the electronic coupling between the donor and acceptor, which depends not only on the donor–acceptor distance, but also

on the electronic properties of the linkers. Thus, the donor–acceptor hybrid molecules with a wide variety of linkers including non-conjugated linkers, such as amides [6,12–15], imides [16], and norbornylogous bridges [17], and π-conjugated linkers, such as oligoynes [18] and oligothiophenes [19], have been synthesized in order to elucidate the influence of the electronic properties of the linkers on the electronic coupling term. These studies have demonstrated that the attenuation factors of the non-conjugated linkers are large, while those of the π-conjugated linkers are small. These cases dealt with mainly carbon-based linkers, and it is of great interest to study the ET through the heavier element-based architecture.

Among the heavy main group element-catenated systems, polysilanes and oligosilanes have been extensively studied because of their potential utilities as charge transport materials and photoconductive materials derived from the high degree of σ-electron delocalization over the silicon framework (σ-conjugation) [20]. One of the most striking features of the oligosilanes is the high sensitivity of their properties to the conformation of the silicon framework. Since the silicon backbones of the oligosilanes are highly flexible due to a small rotational barrier of the Si–Si bond, the elucidation of the structural dependence of their properties requires conformation control in an appropriate manner [21,22]. Our approach for freezing the dynamic behavior of the oligosilanes is based on the incorporation of the disilane or trisilane into the bicyclic framework [21], and these studies have provided clear-cut evidence for the generally accepted idea that the *anti* conformation with large SiSiSiSi dihedral angle (ω) effectively extends the σ-conjugation while *syn* and *cisoid* conformations with a small ω insulate the σ-conjugation.

Very recently, we reported the synthesis of a zinc porphyrin–fullerene dyad linked by 1,2-dialkynyldisilane and investigated their excited-state dynamics. The occurrence of the effective intramolecular photoinduced ET and the generation of the CS state indicates that the disilane moiety works as a molecular wire [23]. The construction of the porphyrin–fullerene dyads linked by conformation-constrained oligosilane chain is of interest for evaluating the influence of the degree of σ-conjugation and the dynamic behavior of the silicon chain on the ET. In this paper, we report the synthesis of the porphyrin–fullerene dyads linked by the conformation-constrained tetrasilane, such as **ZnP–[Si₄(*anti*)]–C₆₀** and **ZnP–[Si₄(*syn*)]–C₆₀**, as well as the permethylated tetrasilane-linked dyad **ZnP–[Si₄]–C₆₀** (Chart 1) to study their excited-state dynamics on the basis of time-resolved fluorescence and absorption measurements.

2. Results and discussion

2.1. Synthesis

Scheme 1 shows the preparation of the tetrasilane moieties. As demonstrated in Scheme 1a, we have developed
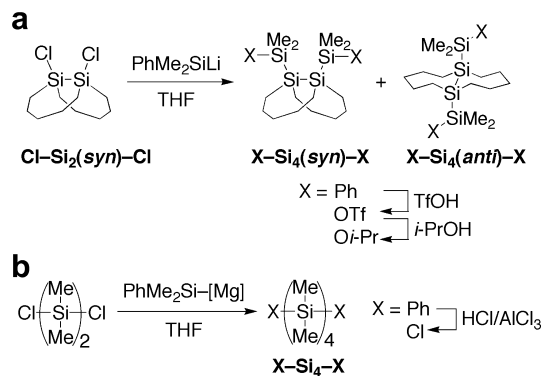
an alternative synthetic route for the conformationally constrained tetrasilanes to the previously reported selective synthesis based on the stereospecific nucleophilic substitution reaction on the silicon center [21a]. Thus, the mixture of the conformation-constrained tetrasilanes **Ph–Si₄(*anti*)–Ph** and **Ph–Si₄(*syn*)–Ph** having phenyl groups on each end of the silicon chain was first prepared by the reaction of a bicyclic dichlorodisilane **Cl–Si₂(*syn*)–Cl** and dimethylphenylsilyllithium [24]. The mixture of the isomers was subjected to the reaction with trifluoromethanesulfonic acid (TfOH) followed by the treatment with 2-propanol to
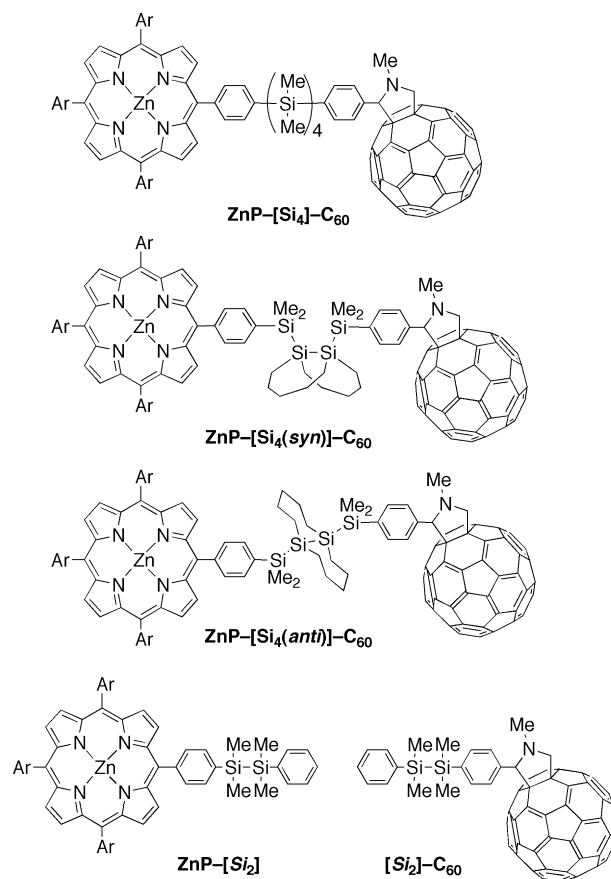

Scheme 1.

Chart 1.

give a mixture of *i*-PrO–**Si₄**(*anti*)–O*i*-Pr and *i*-PrO–**Si₄**(*syn*)–O*i*-Pr with isopropoxy groups on each end. The crystalline *anti*-isomer was obtained in pure form by crystallization of the viscous reaction mixture from toluene/ acetonitrile, while the oily *syn*-isomer was obtained by silica gel column chromatography of the concentrated mother liquor. The configuration of the *anti*-isomer was confirmed by X-ray crystallography (Table 1, Fig. 1). The current procedure is advantageous when both isomers are needed at once and is applicable to the gram-scale preparation of the conformationally constrained tetrasilane units.

Scheme 1b shows the synthesis of the permethylated tetrasilane **Cl**–**Si₄**–**Cl** having chlorine on each end. Thus, the reaction of 1,2-dichlorotetramethyldisilane with the dimethylphenylsilylmagnesium reagent [25] produced **Ph**–**Si₄**–**Ph**, which was dephenylchlorinated with hydrogen chloride in the presence of AlCl₃ to give the target product.

Scheme 2 shows the preparation of the dyads from the obtained tetrasilanes. The chlorine or isopropoxy groups of the tetrasilanes were substituted with *p*-bromophenyl groups using *p*-bromophenyllithium, followed by the transformation of one bromine atom to a formyl group to give
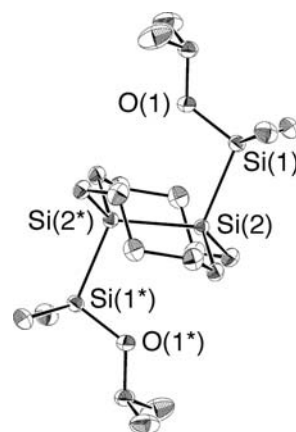

Fig. 1. ORTEP drawing of *i*-PrO–**Si₄**(*anti*)–O*i*-Pr with thermal ellipsoid plot (50% probability). Selected bond lengths (Å) and angles (°): Si(1)–Si(2) 2.3597(12), Si(2)–Si(2*) 2.3588(18), Si(1)–Si(2)–Si(2*) 109.06(3), Si(1)–Si(2)–Si(2*)–Si(1*) 180.

the unsymmetrical tetrasilanes **Br**–[**Si₄**]–**CHO** having a *p*-bromophenyl group on one end and a *p*-formylphenyl group on the other end. Suzuki-Miyaura coupling between the porphyrin boronic ester **ZnP**–**Bpin** and **Br**–[**Si₄**]–**CHO** produced the porphyrin-linked tetrasilanes containing a formyl group **ZnP**–[**Si₄**]–**CHO**. The Prato reaction [26] using C₆₀ and *N*-methylglycine gave the tetrasilane-linked zinc porphyrin–fullerene dyads **ZnP**–[**Si₄**]–**C₆₀**. The products were characterized on the basis of their ¹H, ¹³C, ²⁹Si NMR, and FAB-mass spectra. The reference compounds **ZnP**–[**Si₂**] and [**Si₂**]–**C₆₀** were synthesized in a similar manner.

In the ¹H NMR spectra of the dyads **ZnP**–[**Si₄**]–**C₆₀** and **ZnP**–[**Si₄**(*anti*)]–**C₆₀**, the signals of eight β protons of the ZnP core are shifted upfield by 0.01–0.10 ppm relative to **ZnP**–[**Si₄**]–**CHO** and the porphyrin reference **ZnP**–[**Si₂**]. These spectral perturbations can be understood by the shielding effect of the C₆₀ moiety, and we assumed the existence of a fast equilibrium between two conformers: a folded conformer, in which the ZnP and C₆₀ moieties are proximate to each other, and an extended conformer, in which the ZnP and C₆₀ moieties are separated from each other as shown in Fig. 2. Such an upfield shift of the porphyrin β protons of **ZnP**–[**Si₄**(*syn*)]–**C₆₀** is small relative to **ZnP**–[**Si₄**(*anti*)]–**C₆₀** and **ZnP**–[**Si₄**]–**C₆₀**, suggesting that the folded-extended equilibrium moves to the extended conformer in **ZnP**–[**Si₄**(*syn*)]–**C₆₀**. These assumptions are supported by the semi-empirical calculations (Fig. 2) and photophysical measurements described below.

2.2. Electrochemistry

To estimate the energies of the CS states formed by the photoexcitation, the first oxidation potential (E_{ox}) of the ZnP moiety and the first reduction potential (E_{red}) of the C₆₀ moiety were measured in benzonitrile (BN) using the square-wave voltammetry method in the presence of ferrocene (Fc) as the internal standard. The data are

Table 1
Crystal data and structure refinement for *i*-PrO–**Si₄**(*anti*)–O*i*-Pr

Formula	$C_{20}H_{46}O_2Si_4$
Formula weight	430.93
Temperature (K)	173(2)
Wavelength (Å)	0.71070
Crystal system	Triclinic
Space group	$P\bar{1}$ (#2)
Unit cell dimensions	
a (Å)	7.503(5)
b (Å)	8.992(6)
c (Å)	10.658(7)
α (°)	91.205(7)
β (°)	109.362(8)
γ (°)	106.988(8)
Volume (Å³)	643.2(7)
Z	1
D_{calc} (g/cm³)	1.112
Absorption coefficient (mm⁻¹)	0.243
$F(000)$	238
Crystal size (mm)	$0.50 \times 0.30 \times 0.20$
θ Range for data collection (°)	3.37–27.52
Index ranges	$-9 \leqslant h \leqslant 9$, $-10 \leqslant k \leqslant 11$, $-13 \leqslant l \leqslant 13$
Reflections collected	5092
Independent reflections (R_{int})	2814 (0.0339)
Completeness to $\theta = 27.52°$ (%)	95.0
Maximum and minimum transmission	0.9530 and 0.8881
Refinement method	Full-matrix least-squares on F^2
Data/restraints/parameters	2814/0/202
Goodness-of-fit on F^2	1.037
Final R indices [$I > 2\sigma(I)$]	$R_1 = 0.0318$, $wR_2 = 0.0825$
R indices (all data)	$R_1 = 0.0370$, $wR_2 = 0.0846$
Largest difference in peak and hole (e Å⁻³)	0.346 and −0.208

Scheme 2.

summarized in Table 2. The E_{ox} values of the dyads ZnP–[Si$_4$(*anti*)]–C$_{60}$, ZnP–[Si$_4$(*syn*)]–C$_{60}$, and ZnP–[Si$_4$]–C$_{60}$ are almost the same, while the E_{red} values slightly vary from −1.04 to −1.10 V versus Fc/Fc$^+$. Thus, the ΔE values in Table 2, which denote the energy of the CS states when the distances between ZnP and C$_{60}$ are the same, vary among these three dyads, indicating the existence of the slight interaction between the ZnP and C$_{60}$ moieties in the ground state. From these values, energy levels of the CS states are found to be moderately low, thus the charge separation from the singlet excited state of the ZnP and C$_{60}$ moieties are exothermic paths and can occur.

2.3. Steady-state photophysical measurements

The UV–Vis–NIR absorption spectra of the dyads and the reference compounds measured in BN at room temperature are shown in Fig. 3 and the data are summarized in Table 3. The Soret bands of ZnP–[Si$_4$(*anti*)]–C$_{60}$ and ZnP–[Si$_4$]–C$_{60}$ ($\lambda_{max}^{ABS} = 437.5nm$) show a 6.5 nm red-shift and their extinction coefficients are about a half that of ZnP–[Si$_2$]. The spectra of ZnP–[Si$_4$(*anti*)]–C$_{60}$ and ZnP–[Si$_4$]–C$_{60}$ show the broadened Q bands, as compared to that of ZnP–[Si$_2$], in addition to the weak broad absorption bands close to near-IR region (800–900 nm) where the reference compounds show no or little absorption. On the other hand, such spectral perturbations are somewhat smaller in ZnP–[Si$_4$(*syn*)]–C$_{60}$ than the other dyads. Thus, the Soret band of ZnP–[Si$_4$(*syn*)]–C$_{60}$ ($\lambda_{max}^{ABS} = 433.5nm$) is red-shifted by only 2.5 nm relative to the reference compound ZnP–[Si$_2$], and the absorption band in the near-IR region is slightly weaker than those of ZnP–[Si$_4$(*anti*)]–C$_{60}$ and ZnP–[Si$_4$]–C$_{60}$. These spectral features can be understood by considering the existence of the folded conformers in equilibrium with extended conformers; it is well-known that

the Soret and Q bands of porphyrins are broadened, and a weak broad CT absorption band arises in the NIR region when porphyrins are located close to fullerenes [27]. The weaker perturbation in ZnP–[Si$_4$(*syn*)]–C$_{60}$ than those in ZnP–[Si$_4$(*anti*)]–C$_{60}$ and ZnP–[Si$_4$]–C$_{60}$ is explained by the hindrance of the approach of ZnP to C$_{60}$ in ZnP–[Si$_4$(*syn*)]–C$_{60}$.

Fig. 4 shows the steady-state fluorescence spectra of ZnP–[Si$_4$(*anti*)]–C$_{60}$, ZnP–[Si$_4$(*syn*)]–C$_{60}$, ZnP–[Si$_4$]–C$_{60}$, and ZnP–[Si$_2$] measured in BN at room temperature with excitation at 546 nm, which is one of the isosbestic points of the absorption spectra. The fluorescence quantum yields of the dyads (Φ_{FL}^{Dyad}) and ZnP–[Si$_2$] (Φ_{FL}^{Ref}) were evaluated using zinc tetraphenylporphyrin as a reference as summarized in Table 3 [28]. The shapes of the spectra of the dyads are almost identical to that of the porphyrin reference ZnP–[Si$_2$]. The fluorescence of the C$_{60}$ moiety, which is normally expected to appear around 720 nm upon excitation, was hardly recognized in Fig. 4 due to its low fluorescence quantum yield. The fluorescence intensities of the ZnP moiety of the dyads significantly decreased compared to that of ZnP–[Si$_2$], indicating the occurrence of the quenching of the lowest singlet excited-state of the ZnP by connecting the C$_{60}$ moiety. The order of the fluorescence intensities is ZnP–[Si$_4$(*syn*)]–C$_{60}$ > ZnP–[Si$_4$(*anti*)]–C$_{60}$ > ZnP–[Si$_4$]–C$_{60}$. The fact that the fluorescence intensities of the conformation constrained dyads are higher than that of ZnP–[Si$_4$]–C$_{60}$ can be attributed the suppression effect of the vibrational and rotational non-radiative decay of the excited state in terms of the constraint of the molecular movement by the cyclic structure [29]. The slightly higher fluorescence quantum yield of ZnP–[Si$_4$(*syn*)]–C$_{60}$ than that of ZnP–[Si$_4$(*anti*)]–C$_{60}$ is consistent with the NMR and the absorption spectral measurements that the ZnP–[Si$_4$(*syn*)]–C$_{60}$ has a lower amount of the folded conformer than ZnP–[Si$_4$(*anti*)]–C$_{60}$.

(a) **ZnP**–**[Si$_4$(*anti*)]**–**C$_{60}$** extended; R_{cc}^{ext} = 20.6 Å

(b) **ZnP**–**[Si$_4$(*anti*)]**–**C$_{60}$** folded; R_{cc}^{fol} = 9.9 Å

(c) **ZnP**–**[Si$_4$(*syn*)]**–**C$_{60}$** extended; R_{cc}^{ext} = 22.2 Å

(d) **ZnP**–**[Si$_4$(*syn*)]**–**C$_{60}$** folded; R_{cc}^{fol} = 14.8 Å

(e) **ZnP**–**[Si$_4$]**–**C$_{60}$** extended; R_{cc}^{ext} = 20.6 Å

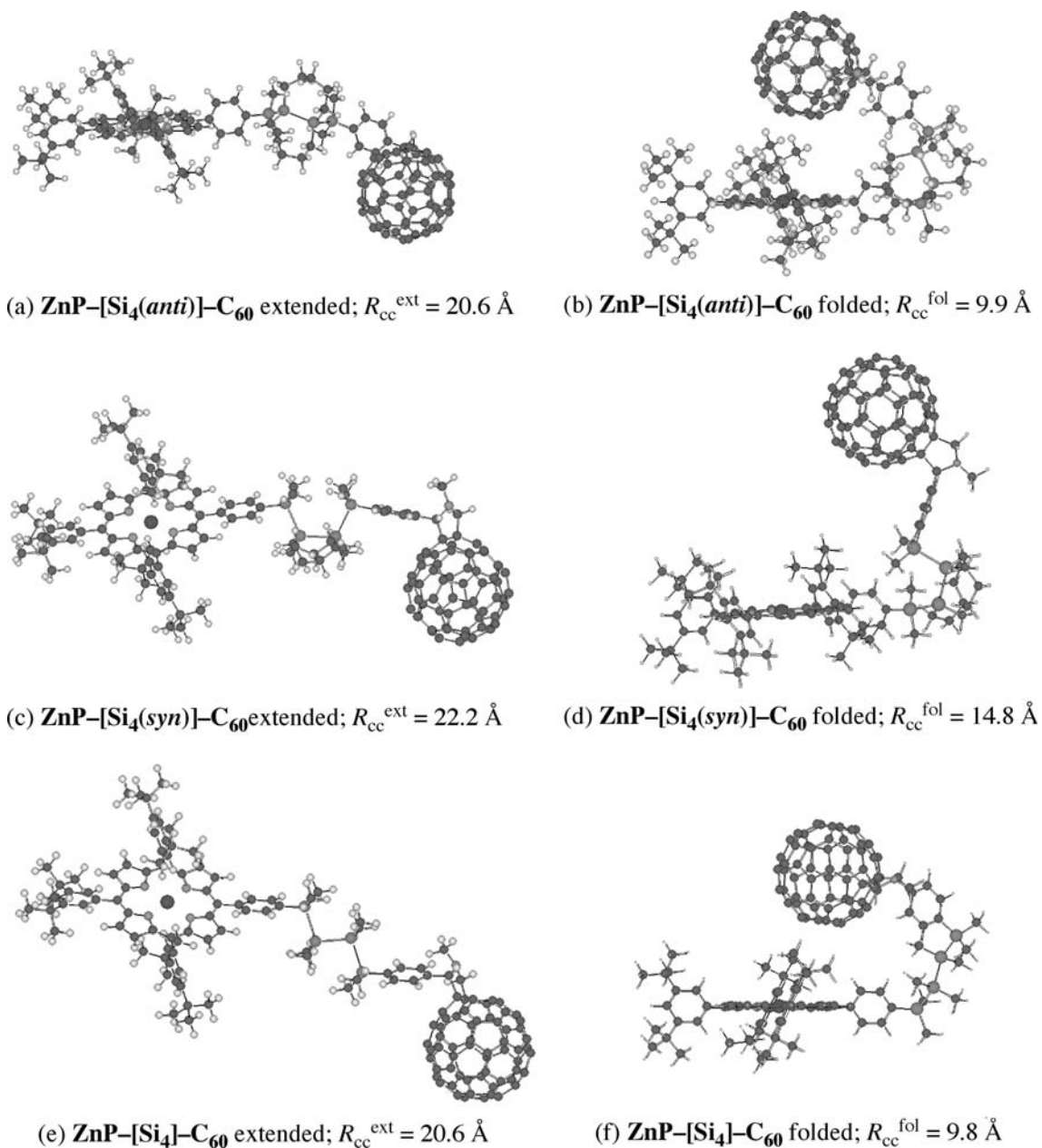(f) **ZnP**–**[Si$_4$]**–**C$_{60}$** folded; R_{cc}^{fol} = 9.8 Å

Fig. 2. Extended and folded conformers of each dyad, together with the center-to-center distances between ZnP and C$_{60}$ moiety (R_{cc}).

Table 2
First oxidation (E_{ox}), reduction potentials (E_{red}), and differences ($\Delta E = E_{ox} - E_{red}$) of the dyads measured in BN

Compound	E_{ox} (V)[a]	E_{red} (V)[a]	ΔE (V)[a]
ZnP–**[Si$_4$(*anti*)]**–**C$_{60}$**	0.27	−1.04	1.31
ZnP–**[Si$_4$(*syn*)]**–**C$_{60}$**	0.27	−1.08	1.35
ZnP–**[Si$_4$]**–**C$_{60}$**	0.27	−1.10	1.37

[a] vs. Fc/Fc$^+$.

2.4. Time-resolved photophysical measurements

The time-resolved fluorescence measurements of the BN solution of the dyads **ZnP**–**[Si$_4$(*anti*)]**–**C$_{60}$**, **ZnP**–**[Si$_4$(*syn*)]**–**C$_{60}$**, and **ZnP**–**[Si$_4$]**–**C$_{60}$**, and the porphyrin reference **ZnP**–**[Si$_2$]** were performed using a time-correlated single-photon
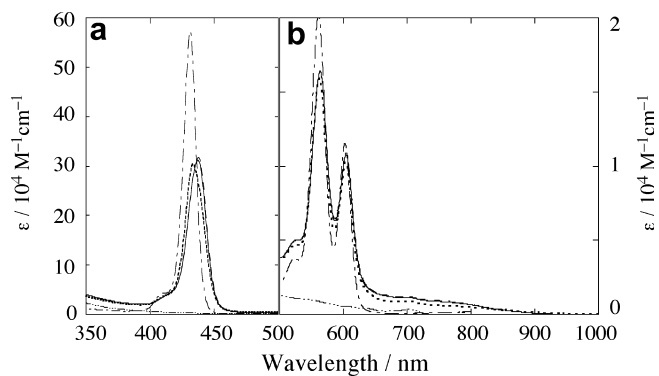
Fig. 3. Steady-state UV–Vis–NIR absorption spectra of **ZnP**–**[Si$_4$(*anti*)]**–**C$_{60}$** (-----), **ZnP**–**[Si$_4$(*syn*)]**–**C$_{60}$** (– – –), **ZnP**–**[Si$_4$]**–**C$_{60}$** (——), **ZnP**–**[Si$_2$]** (–·–·–), and **[Si$_2$]**–**C$_{60}$** (·····) in BN. (a) Soret band region (350–500 nm) and (b) longer wavelength region (500–1000 nm).

Table 3
Steady-state UV–Vis–NIR absorption and fluorescence spectra of the dyads ZnP–[Si$_4$]–C$_{60}$ and the reference compound ZnP–[Si$_2$] in BN

Compound	Absorption	Fluorescence	
	λ_{max}^{ABS} (ε)/nm	λ_{max}^{FL}/nm $(\Phi_{FL})^a$	$\Phi_{FL}^{Dyad}/\Phi_{FL}^{Ref}$
ZnP–[Si$_4$(anti)]–C$_{60}$	437.5 (317000) 563.5 (16400) 604.5 (10900)	609, 660 (1.4 × 10^{-3})	0.025
ZnP–[Si$_4$(syn)]–C$_{60}$	433.5 (303000) 563.0 (15900) 604.5 (10200)	608, 660 (2.0 × 10^{-3})	0.035
ZnP–[Si$_4$]–C$_{60}$	437.5 (312000) 563.5 (16400) 604.5 (10800)	609, 659 (8.7 × 10^{-4})	0.015
ZnP–[Si$_2$]	431.0 (572000) 561.0 (20200) 602.5 (11500)	609, 660 (5.8 × 10^{-2})	–

^{a} Fluorescence quantum yield relative to zinc tetraphenylporphyrin ($\Phi_{FL} = 0.04$).
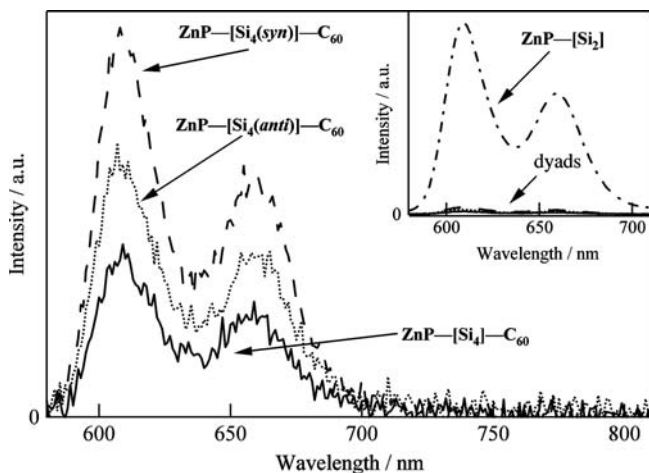
Fig. 4. Steady-state fluorescence spectra of ZnP–[Si$_4$(anti)]–C$_{60}$ (-----), ZnP–[Si$_4$(syn)]–C$_{60}$ (– – –), and ZnP–[Si$_4$]–C$_{60}$ (——) excited by 546 nm light. Inset: Full picture of the fluorescence spectra of the dyads and ZnP–[Si$_2$] (–·–·–).

Fig. 5. Fluorescence time-profile of ZnP moiety of ZnP–[Si$_4$(anti)]–C$_{60}$, ZnP–[Si$_4$(syn)]–C$_{60}$, ZnP–[Si$_4$]–C$_{60}$, and ZnP–[Si$_2$] in BN excited by 400 nm laser light.

Table 4
Fluorescence lifetime (τ_{FL}) and charge-recombination rate (k_{CR}) in BN

Compound	τ_{FL}/ns (fraction/%)^a	$\tau_{FL}^{Dyad}/\tau_{FL}^{Ref}$	k_{CR} (s^{-1})
ZnP–[Si$_4$(anti)]–C$_{60}$	0.40 (77)	0.21	4.3 × 10^6
ZnP–[Si$_4$(syn)]–C$_{60}$	0.32 (70)	0.17	2.9 × 10^6
ZnP–[Si$_4$]–C$_{60}$	0.25 (65)	0.13	2.7 × 10^6
ZnP–[Si$_2$]	1.90 (100)	–	–

^{a} Fitted by bi-exponential function.

ZnP–[Si$_4$(anti)]–C$_{60}$ [30]. The relative τ_{FL} values of the dyads ($\tau_{FL}^{Dyad}/\tau_{FL}^{Ref}$) are higher than the fluorescence quantum yields estimated from the steady-state fluorescence measurements ($\Phi_{FL}^{Dyad}/\Phi_{FL}^{Ref}$) in Table 3 [31]. This inconsistency between these two parameters can be understood by the assumption that the dyads contain a considerable amount of the folded conformers, which immediately transit to the non-fluorescent state, such as exciplex, which is hardly observable in the steady-state fluorescence measurements.

The nanosecond transient absorption spectra of ZnP–[Si$_4$(syn)]–C$_{60}$ in BN are shown in Fig. 6. The other dyads afforded similar spectra. An intense transient absorption band of the C$_{60}$-radical anion was clearly observed around 1000 nm. Although there was breach around 520 nm, the transient absorption band of the ZnP-radical cation was
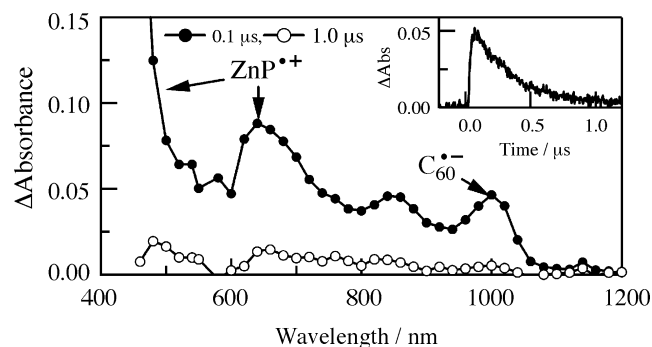
Fig. 6. Nanosecond transient absorption spectra of ZnP–[Si$_4$(syn)]–C$_{60}$ in BN at 0.1 and 1.0 μs. Inset: absorption time-profile at 1000 nm.

counting technique. The fluorescence time-profiles of the ZnP moiety are shown in Fig. 5, and the major components of the lifetimes (τ_{FL}^{Dyad} for the dyads and τ_{FL}^{Ref} for ZnP–[Si$_2$]) fitted by bi-exponential functions are summarized in Table 4. The remarkable shortening of the fluorescence lifetimes of the dyads compared with ZnP–[Si$_2$] indicates the occurrence of the ET and EN from the lowest singlet excited-states of ZnP to C$_{60}$ of the dyads although the involvement of the direct EN is not appreciable in the present case [14]. The multi-component fluorescence decay can be attributed to the fluctuations of the conformers. The order of the fluorescence lifetimes of the dyads is as follows: ZnP–[Si$_4$(anti)]–C$_{60}$ > ZnP–[Si$_4$(syn)]–C$_{60}$ > ZnP–[Si$_4$]–C$_{60}$. The shortest lifetime of ZnP–[Si$_4$]–C$_{60}$ is due to the dynamic behavior of the silicon chain [29], as already discussed. Such a dynamic molecular motion would be also the origin of the shorter lifetime of ZnP–[Si$_4$(syn)]–C$_{60}$ than that of
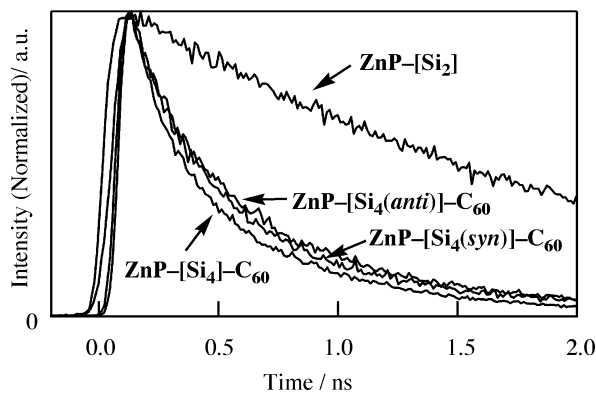
also observed at a wavelength shorter than 700 nm. These absorptions indicate the formation of the radical ion-pair $ZnP^{\cdot+}–[Si_4(syn)]–C_{60}^{\cdot-}$ by the intramolecular charge separation. The charge-recombination rates (k_{CR}) of the dyads estimated by the decay rate of the transient absorption at 1000 nm are summarized in Table 4. The k_{CR} of the dyads slightly depend on the linkage conformation: **ZnP–[Si₄-(anti)]–C₆₀ > ZnP–[Si₄(syn)]–C₆₀ > ZnP–[Si₄]–C₆₀**, which shows an opposite tendency to that of the $1/\tau_{FL}^{Dyad}$ values. Although the mechanism of the charge-recombination process is not clear at the present stage, this result is suggestive of the existence of the superexchange mechanism in the back ET through the Si-linkage and a competitive charge-recombination path, such as a direct back ET by the intramolecular collision of the radical ion centers based on the molecular motion.

3. Conclusion

Zinc porphyrin–fullerene dyads linked by the conformation-constrained tetrasilanes were synthesized together with the permethylated tetrasilane-linked dyad. Time-resolved fluorescence measurements revealed that the ET occur on a sub-nanosecond to nanosecond timescale. The transient absorption spectra in polar solvents are mainly composed of the C_{60}-radical anion and the ZnP-radical cation, indicating the generation of the CS state with a sub-microsecond lifetime. The lifetimes of the CS states hardly depend on the conformation of the tetrasilane linkers. These observations imply that the CR rate show little dependence on the degree of σ-conjugation. This is in sharp contrast to the π-conjugated linkers, which show the unambiguous linkage dependence of the ET rates [13]. Such a difference would be one of the characteristics of the silicon linkage. The clarification of the dependence of the ET rates on the number of silicon atoms in the oligosilane linkers are currently being performed in our laboratories.

4. Experimental

4.1. General

Melting points (mp) were determined with a Yanaco MP-S3 instrument and are uncorrected. ¹H and ¹³C NMR spectra were recorded on a Varian Mercury (300 MHz for ¹H) and JEOL EX-270 (67.94 MHz for ¹³C) spectrometer in C_6D_6 unless otherwise stated and chemical shifts are reported in δ ppm with reference to internal solvent peak for ¹H (C_6HD_5: 7.20 ppm) and ¹³C (C_6D_6: 128.0 ppm), respectively. ²⁹Si NMR spectra were recorded with JEOL EX-270 (59.62 MHz for ²⁹Si) spectrometer in C_6D_6 with the use of the proton-decoupled INEPT technique using tetramethylsilane (0.0 ppm) as an external standard. Recycle preparative gel permeation chromatography (GPC) was performed using polystyrene gel columns (JAIGEL 1H and 2H, LC-908, Japan Analytical Industry) with toluene as an eluent. Column chromatography was performed using

Kieselgel 60 (70-230 mesh, Merck) unless otherwise stated. All reactions were carried out under nitrogen unless otherwise stated. All dry solvents were freshly distilled under N_2 before use. THF, Et_2O, and DME were distilled from sodium/benzophenone. Benzene and toluene were distilled from sodium. CH_2Cl_2 was distilled from CaH_2. Acetone was distilled from anhydrous K_2CO_3. Hexane was distilled from sodium/benzophenone/triglym. 1,7-Dichloro-1,7-disilabicyclo[5.5.0]dodecane [21a], 1,2-dichloro-1,1,2,2-tetramethyldisilane [32], 1-(4-bromophenyl)-1,1,2,2-tetramethyl-2-phenyldisilane [33], [5-(4,4,5,5-tetramethyl-1,3,2-dioxaborolan-2-yl)-10,15,20-tris[3′,5′-(di-*tert*-butyl)phen-yl]porphinato]zinc(II) (**ZnP–Bpin**) [34], and **[Si₂]–C₆₀** [23] were synthesized as described before.

4.2. anti- and syn-1,7-Isopropoxydimethylsilyl-1,7-disilabicyclo[5.5.0]dodecane (*i-PrO–Si₄(anti)–O-i-Pr* and *i-PrO–Si₄(syn)–Oi-Pr*)

To a solution of 1,7-dichloro-1,7-disilabicyclo[5.5.0]dodecane (**Cl–Si₂(syn)–Cl**; 2.35 g, 8.78 mmol) in THF (10 mL) was added a solution of dimethylphenylsilyllithium, which was prepared from lithium (granular, 512 mg, 73.7 mmol) and chlorodimethylphenylsilane (3.0 mL, 18.1 mmol) in THF (20 mL), dropwise over 10 min at 0 °C. Upon completion of the addition, the reaction mixture was allowed to warm to room temperature. After being stirred for 2 h, the resulting mixture was quenched with H_2O (20 mL) and evaporated to remove THF. To the residue was added Et_2O (20 mL). The resulting biphasic mixture was separated and the aqueous layer was extracted with Et_2O (3 × 20 mL). The combined organic layer was washed with brine (40 mL) and dried over $MgSO_4$. After filtration and evaporation, the residue was subjected to silica gel column chromatography (hexane, $R_f = 0.32$) to give 3.09 g (6.62 mmol, 75% yield) of a mixture of *anti*- and *syn*-1,7-dimethylphenylsilyl-1,7-disilabicyclo[5.5.0]dodecanes (**Ph–Si₄(anti)–Ph** and **Ph–Si₄(syn)–Ph**) as white solids (*syn/anti* = 1.7/1). This mixture was used for the next reaction without separating the isomers.

To a solution of the mixture of **Ph–Si₄(anti)–Ph** and **Ph–Si₄(syn)–Ph** (3.09 g, 6.62 mmol) in CH_2Cl_2 (16 mL) was added TfOH (1.2 mL, 13.6 mmol) dropwise over 5 min at 0 °C. Upon completion of the addition, the reaction mixture was stirred for 1 h. To this mixture was added 2,6-lutidine (3.1 mL, 26.7 mmol) in one portion and added a solution of isopropyl alcohol (1.5 mL, 19.6 mmol) in CH_2Cl_2 (5 mL) dropwise over 5 min at 0 °C. Upon completion of the addition, the reaction mixture was allowed to warm to room temperature and stirred for 2 h. To this mixture was added H_2O (20 mL). The resulting biphasic mixture was separated and the aqueous layer was extracted with Et_2O (3 × 20 mL). The combined organic layer was washed with brine (30 mL) and dried over $MgSO_4$. After filtration and evaporation, the residue was subjected to silica gel column chromatography (Silica Gel 60 N (spherical, neutral), Kanto Chemical Co., Inc, hexane/Et_3N = 100/1,

$R_f = 0.07$–0.15) to give 2.50 g (5.80 mmol, 88% yield) of a mixture of *anti*- and *syn*-1,7-isopropoxydimethylsilyl-1,7-disilabicyclo[5.5.0]dodecane (*i*-PrO–**Si₄**(*anti*)–O*i*-Pr and *i*-PrO–**Si₄**(*syn*)–O*i*-Pr) as a colorless oil (*syn/anti* = 1.6/1).

Isomers were separated by neutralized silica gel column chromatography (PSQ 100B, Fuji Silysia, hexane/AcOEt = 100/1) and recrystallization from toluene/acetonitrile. *i*-PrO–**Si₄**(*anti*)–O*i*-Pr: colorless crystals. Mp 72–73 °C. ^{1}H NMR (C₆D₆): $\delta = 3.94$ (sept, $J = 6.0$ Hz, 2H), 1.82–2.04 (m, 8H), 1.62–1.69 (m, 4H), 1.26 (ddd, $J = 13.9$, 8.5, 5.2 Hz, 4H), 1.16 (d, $J = 6.0$ Hz, 12H), 1.02 (ddd, $J = 13.9$, 8.5, 5.2 Hz, 4H), 0.47 (s, 12H). ^{13}C NMR (C₆D₆): $\delta = 65.57$, 31.05, 28.05, 26.36, 12.90, 2.60. ^{29}Si NMR (C₆D₆): $\delta = 14.48$, -30.43. HRMS(EI): Calc. for C₂₀H₄₆O₂Si₄: 430.2575. Found: 430.2594. *i*-PrO–**Si₄**(*syn*)–O*i*-Pr: colorless oil. ^{1}H NMR (C₆D₆): $\delta = 3.97$ (sept, $J = 6.0$ Hz, 2H), 1.79–1.87 (m, 8H), 1.64–1.71 (m, 4H), 1.19 (d, $J = 6.0$ Hz, 12H), 0.95–1.14 (m, 8H), 0.49 (s, 12H). ^{13}C NMR (C₆D₆): $\delta = 65.70$, 33.09, 26.42, 23.95, 11.53, 1.87. ^{29}Si NMR (C₆D₆): $\delta = 14.08$, -38.70. HRMS(EI): Calc. for C₂₀H₄₆O₂Si₄: 430.2575. Found: 430.2589.

4.3. 1,4-Dichloro-1,1,2,2,3,3,4,4-octamethyltetrasilane (Cl–Si₄–Cl)

To a suspension of lithium (granular, 1.66 g, 239 mmol) and THF (50 mL) was added a solution of chlorodimethylphenylsilane (10.0 mL, 60.5 mmol) in THF (10 mL) dropwise over 20 min at 0 °C. After being stirred for 4 h, the resulting mixture was filtered to remove excess lithium. To this silyllithium solution was added 60 mL (60.6 mmol) of a 1.01 M solution of isopropylmagnesium bromide in Et₂O dropwise over 20 min at 0 °C to give a silylmagnesium reagent.

To a solution of 1,2-dichloro-1,1,2,2-tetramethyldisilane (5.65 g, 30.2 mmol) in THF (30 mL) was added the solution of thus prepared silylmagnesium reagent dropwise over 20 min at 0 °C. Upon completion of the addition, the reaction mixture was allowed to warm to room temperature. After being stirred for 8 h, the reaction mixture was quenched with saturated aq. NH₄Cl (20 mL) and H₂O (40 mL). The resulting biphasic mixture was separated and the aqueous layer was extracted with Et₂O (3 × 50 mL). The combined organic layer was washed with brine and dried over MgSO₄. After filtration and evaporation, the residue was subjected to silica gel column chromatography (hexane, $R_f = 0.33$) to give 7.19 g (18.6 mmol, 62% yield) of 1,1,2,2,3,3,4,4-octamethyl-1,4-diphenyltetrasilane [35] as white solids. ^{1}H NMR (C₆D₆): $\delta = 7.46$–7.49 (m, 4H), 7.2–7.3 (m, 6H), 0.39 (s, 12H), 0.16 (s, 12H).

To a solution of 1,1,2,2,3,3,4,4-octamethyl-1,4-diphenyltetrasilane (6.39 g, 16.5 mmol) in benzene (20 mL) was added AlCl₃ (66.2 mg, 0.497 mmol), and then HCl gas was blown on this mixture for 3 h at room temperature. Hexane (20 mL) and acetone (1 mL) were added and the resulting acetone/AlCl₃ complex was filtered off. Evaporation followed by distillation at reduced pressure (190–195 °C/13 mmHg) gave 4.44 g (14.6 mmol, 89% yield) of 1,4-dichloro-1,1,2,2,3,3,4,4-octamethyltetrasilane [36] (**Cl–Si₄–Cl**) as colorless oil. ^{1}H NMR (C₆D₆): $\delta = 0.44$ (s, 12H), 0.24 (s, 12H).

4.4. Conversion from X–Si₄–X (X = Cl or i-PrO) to Br–[Si₄]–Br

4.4.1. A typical procedure: 1,4-bis(4-bromophenyl)-1,1,2,2,3,3,4,4-octamethyltetrasilane (Br–[Si₄]–Br)

To a suspension of *p*-dibromobenzene (4.79 g, 20.3 mmol) in Et₂O (20 mL) was added 12.8 mL (20.0 mmol) of a 1.56 M solution of *n*-butyllithium in hexane dropwise over 10 min at -78 °C. Upon completion of addition, the reaction mixture was allowed to warm to room temperature and stirred for 2.5 h to give a suspension of *p*-bromophenyllithium in Et₂O.

To a suspension of *p*-bromophenyllithium in Et₂O was added a solution of **Cl–Si₄–Cl** (1.54 g, 5.07 mmol) in Et₂O (15 mL) dropwise over 10 min at -78 °C. Upon completion of addition, the reaction mixture was allowed to warm to room temperature and stirred for 1.5 h. To the resulting mixture was added 5% aq. NH₄Cl (40 mL). The resulting biphasic mixture was separated and the aqueous layer was extracted with Et₂O (3 × 40 mL). The combined organic layer was washed with brine (40 mL) and dried over MgSO₄. After filtration and evaporation, the residue was subjected to silica gel column chromatography (hexane, $R_f = 0.43$) to give 2.26 g (4.15 mmol, 82% yield) of **Br–[Si₄]–Br** as pale yellow oil. The product contained some impurities but was used for the next reaction without further purification. ^{1}H NMR (C₆D₆): $\delta = 7.40$ (d, $J = 8.1$ Hz, 4 H), 7.10 (d, $J = 8.1$ Hz, 4H), 0.28 (s, 12H), 0.06 (s, 12H). ^{13}C NMR (C₆D₆): $\delta = -5.34$, -2.82, 123.71, 131.28, 135.55, 138.52. ^{29}Si NMR (C₆D₆): $\delta = -44.28$, -17.31. HRMS(EI): Calc. for C₂₀H₃₂Br₂Si₄: 541.9948. Found: 541.9955.

4.4.2. anti-1,7-Bis(4-bromophenyl)-1,7-disilabicyclo[5.5.0]dodecane (Br–[Si₄(anti)]–Br)

Yield: 91% (white solids). Mp 97.5–98 °C. ^{1}H NMR (C₆D₆): $\delta = 7.41$ (d, $J = 8.1$ Hz, 4H), 7.16 (d, $J = 8.1$ Hz, 4H), 1.42–1.51 (m, 8H), 1.21–1.27 (m, 4H), 0.95 (dt, $J = 14.4$, 6.9 Hz, 4H), 0.64 (dt, $J = 14.4$, 6.9 Hz, 4H), 0.44 (s, 12H). ^{13}C NMR (C₆D₆): $\delta = 139.50$, 135.82, 131.16, 123.56, 30.78, 27.72, 13.32, -0.88. ^{29}Si NMR (C₆D₆): $\delta = -16.68$, -28.43. HRMS(EI): Calc. for C₂₆H₄₀Br₂Si₄: 622.0574. Found: 622.0562.

4.4.3. syn-1,7-Bis(4-bromophenyl)-1,7-disilabicyclo[5.5.0]dodecane (Br–[Si₄(syn)]–Br)

Yield: 69% (white solids). ^{1}H NMR (C₆D₆): $\delta = 7.42$ (d, $J = 8.1$ Hz, 4H), 7.16 (d, $J = 8.1$ Hz, 4H), 1.40–1.60 (m, 12H), 0.75–0.80 (m, 8H), 0.35 (s, 12H). ^{13}C NMR (C₆D₆): $\delta = 138.75$, 135.73, 131.28, 123.76, 32.84, 23.51, 11.51, -1.85. ^{29}Si NMR (C₆D₆): $\delta = -17.93$, -35.57. HRMS(EI): Calc. for C₂₆H₄₀Br₂Si₄: 622.0574. Found: 622.0573.

4.5. Conversion from Br–[Si₄]–Br to Br–[Si₄]–CHO

4.5.1. A typical procedure: 1-(4-bromophenyl)-4-(4-formylphenyl)-1,1,2,2,3,3,4,4-octamethyltetrasilane (Br–[Si₄]–CHO)

To a solution of **Br–[Si₄]–Br** (2.13 g, 3.91 mmol) in THF (16 mL) was added 2.5 mL (4.00 mmol) of a 1.56 M solution of *n*-butyllithium in hexane dropwise over 5 min at −78 °C. Upon completion of addition, the reaction mixture was stirred for 1 h at this temperature to give a white suspension. To this suspension was added a solution of *N*-formylpiperidine (0.65 mL, 5.64 mmol) in THF (8 mL) dropwise over 5 min at −78 °C. After being stirred for 20 min, the reaction mixture was allowed to warm to room temperature and stirred for 45 min. To the resulting clear solution was added 1 N aq. HCl (30 mL). The resulting biphasic mixture was evaporated to remove THF. To the residue was added Et₂O (60 mL). The resulting biphasic mixture was separated and the aqueous layer was extracted with Et₂O (3 × 30 mL). The combined organic layer was washed with brine (50 mL) and dried over MgSO₄. After filtration and evaporation, the residue was subjected to silica gel column chromatography (hexane/toluene = 1/1 to toluene, then toluene/AcOEt = 10/1, R_f = 0.58 (toluene)) to give 781 mg (1.58 mmol, 40% yield (containing small amount of impurities)) of **Br–[Si₄]–CHO** as a pale yellow paste. ¹H NMR (C₆D₆): δ = 9.76 (s, 1H), 7.65 (d, J = 8.1 Hz, 2H), 7.40 (d, J = 8.1 Hz, 2H), 7.38 (d, J = 8.1 Hz, 2H), 7.10 (d, J = 8.1 Hz, 2H), 0.30 (s, 6H), 0.28 (s, 6H), 0.06 (s, 6H), 0.05 (s, 6H). ¹³C NMR (C₆D₆): δ = 191.32, 148.11, 138.42, 136.99, 135.54, 134.29, 131.31, 128.68, 123.76, −2.87, −3.05, −5.37 (one peak is overlapped). ²⁹Si NMR (C₆D₆): δ = −17.01, −17.31, −43.91, −44.08. HRMS(EI): Calc. for C₂₁H₃₃BrOSi₄: 492.0792. Found: 492.0793.

4.5.2. anti-1-(4-Bromophenyl)-7-(4-formylphenyl)-1,7-disilabicyclo[5.5.0]dodecane (Br–[Si₄(anti)]–CHO)

Yield: 39% (white solids). Mp 125–127 °C. ¹H NMR (C₆D₆): δ = 9.75 (s, 1H), 7.65 (d, J = 8.1 Hz, 2H), 7.44 (d, J = 8.1 Hz, 2H), 7.41 (d, J = 8.1 Hz, 2H), 7.15 (d, J = 8.1 Hz, 2H), 1.41–1.48 (m, 8H), 1.20–1.27 (m, 4H), 0.90–1.01 (m, 4H), 0.60–0.69 (m, 4H), 0.46 (s, 6H), 0.44 (s, 6H). ¹³C NMR (C₆D₆): δ = 191.34, 149.19, 139.40, 136.82, 135.80, 134.55, 131.19, 128.58, 123.59, 30.78, 27.72, 27.69, 13.31, −0.89, −1.06 (one peak is overlapped). ²⁹Si NMR (C₆D₆): δ = −16.38, −16.66, −28.03, −28.30. HRMS(EI): Calc. for C₂₇H₄₁BrOSi₄: 572.1418. Found: 572.1408.

4.5.3. syn-1-(4-Bromophenyl)-7-(4-formylphenyl)-1,7-disilabicyclo[5.5.0]dodecane (Br–[Si₄(syn)]–CHO)

Yield: 36% (white waxy solids). ¹H NMR (C₆D₆): δ = 9.79 (s, 1H), 7.66 (d, J = 8.1 Hz, 2H), 7.44 (d, J = 8.1 Hz, 2H), 7.42 (d, J = 8.1 Hz, 2H), 7.17 (d, J = 8.1 Hz, 2H), 1.4–1.7 (m, 12H), 0.7–0.8 (m, 8H), 0.37 (s, 6H), 0.35 (s, 6H). ¹³C NMR (C₆D₆): δ = 191.37, 148.37, 138.65, 136.95, 135.72, 134.45, 131.29, 128.64, 123.79, 32.81, 23.46, 11.45, −1.85, −2.06 (two peaks are overlapped). ²⁹Si NMR (C₆D₆): δ = −17.61, −17.96, −35.29, −35.49. HRMS(EI): Calc. for C₂₇H₄₁BrOSi₄: 572.1418. Found: 572.1408.

4.6. Preparation of ZnP–[Si₄]–CHO

4.6.1. A typical procedure: ZnP–[Si₄]–CHO

A mixture of **Br–[Si₄]–CHO** (781 mg, 1.58 mmol) and **ZnP–Bpin** (151 mg, 0.142 mmol) in DME (40 mL) and H₂O (0.8 mL) was deoxgenized by bubbling with nitrogen for 30 min. To this mixture were added tetrakis(triphenylphosphine)palladium(0) (45.5 mg, 0.0394 mmol) and Ba(OH)₂ · 8H₂O (501 mg, 1.59 mmol). The resulting mixture was warmed to 80 °C and stirred for 20 min. After cooling, the resulting mixture was filtered through a pad of silica gel and washed with CH₂Cl₂. After evaporation, the residue was subjected to silica gel column chromatography (hexane/toluene = 2/1 to 1/3, R_f = 0.70 (hexane/toluene = 1/4)) and subjected to GPC (toluene as an eluent, t_R = 72 min) to give 96.2 mg (0.0712 mmol, 50% yield) of **ZnP–[Si₄]–CHO** as purple solids. ¹H NMR (C₆D₆): δ = 9.72 (s, 1H), 9.33–9.36 (m, 6H), 9.24 (d, J = 4.8 Hz, 2H), 8.46–8.47 (m, 6H), 8.41 (d, J = 7.8 Hz, 2H), 8.03–8.04 (m, 3H), 7.85 (d, J = 8.1 Hz, 2H), 7.67 (d, J = 8.1 Hz, 2H), 7.49 (d, J = 7.8 Hz, 2H), 1.55 (m, 54H), 0.65 (s, 6H), 0.43 (s, 6H), 0.33 (s, 6H), 0.27 (s, 6H). ¹³C NMR (C₆D₆): δ = 191.39, 151.05, 150.99, 150.94, 150.53, 149.03, 144.27, 143.12, 138.38, 136.84, 134.53, 134.35, 132.62, 132.53, 132.31, 132.16, 130.39, 130.32, 128.72, 122.78, 122.73, 121.06, 35.32, 32.03, −2.51, −2.82, −5.01, −5.17. ²⁹Si NMR (C₆D₆): δ = −16.88, −17.53, −43.58 (one peak is overlapped). FAB-MS: 1350 ([M+H]⁺).

4.6.2. ZnP–[Si₄(anti)]–CHO

Yield: 30% (purple solids). ¹H NMR (C₆D₆): δ = 9.78 (s, 1H), 9.38 (d, J = 4.8 Hz, 2H), 9.32–9.35 (m, 4H), 9.26 (d, J = 4.8 Hz, 2H), 8.46–8.47 (m, 6H), 8.40 (d, J = 8.1 Hz, 2H), 8.03–8.04 (m, 3H), 7.89 (d, J = 8.1 Hz, 2H), 7.70 (d, J = 8.1 Hz, 2H), 7.53 (d, J = 8.1 Hz, 2H), 1.6–1.8 (m, 8H), 1.55 (s, 54H), 1.22–1.40 (m, 4H), 1.05–1.17 (m, 4H), 0.80–0.96 (m, 4H), 0.80 (s, 6H), 0.56 (s, 6H). ¹³C NMR (CS₂): δ = 189.87, 150.86, 150.41, 149.72, 148.68, 143.73, 142.61, 139.24, 136.95, 134.94, 134.76, 132.85, 132.74, 132.33, 131.87, 130.53, 129.58, 128.94, 127.38, 122.77, 121.42, 121.14, 35.56, 32.66, 31.69, 28.73, 28.66, 14.43, 14.26, 0.06, −0.12. ²⁹Si NMR (C₆D₆): δ = −15.98, −16.66, −27.38 (one peak is overlapped). FAB-MS: 1430 ([M+H]⁺).

4.6.3. ZnP–[Si₄(syn)]–CHO

Yield: 33% (purple solids). ¹H NMR (C₆D₆): δ = 9.69 (s, 1H), 9.34–9.38 (m, 6H), 9.27 (d, J = 4.8 Hz, 2H), 8.47–8.48 (m, 6H), 8.43 (d, J = 8.1 Hz, 2H), 8.03–8.04 (m, 3H), 7.92 (d, J = 8.1 Hz, 2H), 7.69 (d, J = 8.1 Hz, 2H), 7.55 (d,

$J = 8.1$ Hz, 2H), 1.6–1.9 (m, 12H), 1.55 (s, 54H), 1.0–1.2 (m, 4H), 0.84–0.92 (m, 4H), 0.71 (s, 6H), 0.56 (s, 6H). ^{13}C NMR (C_6D_6): $\delta = 191.45$, 151.04, 150.97, 150.91, 150.51, 148.98, 148.73, 144.29, 143.14, 138.47, 136.80, 134.52, 132.61, 132.53, 132.20, 130.39, 130.34, 128.69, 127.84, 122.75, 122.70, 121.02, 35.31, 32.96, 32.00, 23.72, 23.64, 11.93, 11.60, −1.47, −1.80. ^{29}Si NMR (C_6D_6): $\delta = -17.41$, −18.01, −34.97, −35.19. FAB-MS: 1430 ([M+H]$^+$).

4.7. Preparation of **ZnP–[Si₄]–C₆₀**

4.7.1. A typical procedure: **ZnP–[Si₄]–C₆₀**

A solution of **ZnP–[Si₄]–CHO** (81.7 mg, 0.0605 mmol), C_{60} (216 mg, 0.300 mmol), and *N*-methylglycine (275 mg, 3.06 mmol) in toluene (300 mL) was deoxygenized by bubbling with nitrogen for 30 min and heated under reflux. After being stirred for 10 h in the dark at this temperature, the reaction mixture was allowed to cool to room temperature and filtered through a pad of silica gel. After evaporation, the residue was subjected to silica gel column chromatography (hexane/toluene = 4/1 to 2/3, $R_f = 0.65$ (hexane/toluene = 1/1)) followed by preparative GPC (toluene as an eluent, $t_R = 73$ min). After evaporation, the residue was washed with MeOH to give 100 mg (0.0477 mmol, 79% yield) of **ZnP–[Si₄]–C₆₀** as dark purple solids. ^{1}H NMR (C_6D_6): $\delta = 9.33$ (m, 4H), 9.27 (d, $J = 4.8$ Hz, 2H), 9.16 (d, $J = 4.8$ Hz, 2H), 8.59 (d, $J = 1.8$ Hz, 2H), 8.53 (d, $J = 1.8$ Hz, 4H), 8.35 (d, $J = 8.1$ Hz, 2H), 8.07 (t, $J = 1.8$ Hz, 1H), 8.04 (t, $J = 1.8$ Hz, 2H), 7.77 (d, $J = 8.1$ Hz, 2H), 7.42 (d, $J = 8.1$ Hz, 2H), 4.33 (s, 1H), 4.19 (d, $J = 9.3$ Hz, 1H), 3.45 (d, $J = 9.3$ Hz, 1H), 2.46 (s, 3H), 1.63 (s, 18H), 1.61 (s, 18H), 1.60 (s, 18H), 0.65 (s, 3H), 0.64 (s, 3H), 0.46 (s, 3H), 0.46 (s, 3H), 0.38 (s, 6H), −0.13 (s, 3H), −0.16 (s, 3H) (two aromatic protons are overlapped with the solvent peak). ^{13}C NMR (C_6D_6): $\delta = 155.66$, 153.03, 152.70, 151.05, 150.94, 150.82, 150.44, 149.03, 148.98, 146.07, 145.72, 145.44, 145.25, 144.85, 144.60, 144.55, 144.49, 144.46, 144.36, 144.24, 143.90, 143.83, 143.67, 143.58, 143.47, 143.17, 142.97, 142.81, 142.60, 141.90, 141.69, 141.39, 141.28, 141.18, 141.03, 140.85, 140.82, 140.46, 140.39, 140.26, 140.23, 140.14, 139.96, 139.93, 139.27, 139.24, 138.94, 138.78, 138.22, 137.48, 135.98, 135.83, 135.49, 134.85, 134.70, 134.04, 132.69, 132.54, 132.48, 132.36, 130.44, 130.29, 128.79, 122.93, 122.85, 121.50, 121.02, 83.11, 77.01, 69.40, 68.53, 39.65, 35.39, 32.15, −2.77, −2.82, −2.85, −4.89, −5.40, −5.58. ^{29}Si NMR (C_6D_6): $\delta = -16.61$, −17.41, −43.23, −44.48. FAB-MS: 2097 ([M+H]$^+$).

4.7.2. **ZnP–[Si₄(anti)]–C₆₀**

Yield: 67% (dark purple solids). ^{1}H NMR (C_6D_6): $\delta = 9.30$–9.34 (m, 6H), 9.16 (d, $J = 4.8$ Hz, 2H), 8.52–8.56 (m, 6H), 8.34 (d, $J = 8.1$ Hz, 2H), 8.03–8.06 (m, 3H), 7.81 (d, $J = 8.1$ Hz, 2H), 7.52 (d, $J = 8.1$ Hz, 2H), 4.19 (s, 1H), 4.09 (d, $J = 9.3$ Hz, 1H), 3.28 (d, $J = 9.3$ Hz, 1H), 2.45 (s, 3H), 1.63–1.82 (m, 8H), 1.63 (s, 18H), 1.62 (s, 36H), 1.2–1.6 (m, 12H), 0.76 (s, 3H), 0.74 (s, 3H), 0.65

(s, 3H), 0.63 (s, 3H) (two aromatic protons are overlapped with the solvent peak). ^{13}C NMR (C_6D_6): $\delta = 155.76$, 153.04, 152.78, 151.07, 150.94, 150.86, 150.48, 149.03, 146.18, 145.94, 145.54, 145.44, 145.41, 145.23, 144.87, 144.60, 144.55, 144.50, 144.42, 144.37, 143.98, 143.73, 143.62, 143.53, 143.50, 143.45, 143.19, 143.04, 142.78, 142.68, 141.90, 141.67, 141.48, 141.43, 141.26, 141.16, 141.11, 141.08, 140.98, 140.84, 140.57, 140.51, 140.41, 140.24, 140.18, 140.03, 139.27, 139.01, 138.93, 137.41, 136.13, 135.90, 135.44, 134.91, 134.70, 132.84, 132.74, 132.41, 130.48, 130.40, 130.30, 128.36, 128.00, 127.64, 122.90, 121.65, 121.09, 83.18, 77.02, 69.34, 68.58, 39.64, 35.39, 32.15, 31.03, 30.91, 28.13, 28.00, 27.90, 13.85, 13.19, −0.50, −0.61, −0.98, −1.01. ^{29}Si NMR (C_6D_6): $\delta = -16.61$, −27.28, −28.35 (one peak is overlapped). FAB-MS: 2177 ([M+H]$^+$).

4.7.3. **ZnP–[Si₄(syn)]–C₆₀**

Yield: 77% (dark purple solids). ^{1}H NMR (C_6D_6): $\delta = 9.31$ (d, $J = 4.5$ Hz, 2H), 9.25–9.28 (m, 6H), 8.48–8.50 (m, 2H), 8.45 (d, $J = 1.5$ Hz, 4H), 8.37 (d, $J = 7.8$ Hz, 2H), 8.02–8.05 (m, 3H), 7.95 (d, $J = 7.8$ Hz, 2H), 7.59–7.64 (m, 2H), 4.05–4.08 (m, 2H), 3.27 (d, $J = 9.0$ Hz, 1H), 2.50 (s, 3H), 1.62–1.88 (m, 12H), 1.60 (s, 36H), 1.57 (s, 18H), 1.04–1.16 (m, 4H), 0.8–1.0 (m, 4H), 0.74 (s, 3H), 0.73 (s, 3H), 0.58 (s, 3H), 0.54 (s, 3H) (two aromatic protons are overlapped with the solvent peak). ^{13}C NMR (C_6D_6): $\delta = 155.35$, 152.98, 152.42, 150.91, 150.87, 150.74, 150.43, 149.01, 146.36, 145.97, 145.67, 145.31, 145.20, 145.11, 145.02, 144.92, 144.65, 144.49, 144.36, 144.26, 144.16, 144.11, 144.01, 143.85, 143.73, 143.48, 143.37, 143.12, 143.06, 141.99, 141.76, 141.72, 141.64, 141.38, 141.26, 141.20, 141.10, 141.03, 140.98, 140.92, 140.84, 140.75, 140.59, 140.42, 140.24, 139.01, 138.96, 138.93, 138.86, 138.60, 137.56, 136.21, 135.47, 134.93, 134.60, 134.29, 132.92, 132.72, 132.64, 132.41, 130.47, 130.39, 130.24, 128.94, 122.88, 122.75, 121.32, 121.07, 83.09, 76.71, 69.34, 68.38, 39.78, 35.39, 32.91, 32.17, 30.34, 13.89, 12.25, 12.12, 12.01, −1.11, −1.19, −1.42, −1.57. ^{29}Si NMR (C_6D_6): $\delta = -17.33$, −17.88, −35.34 (one peak is overlapped). FAB-MS: 2177 ([M+H]$^+$).

4.8. Synthesis of **ZnP–[Si₂]**

A solution of 1-(4-bromophenyl)-1,1,2,2-tetramethyl-2-phenyldisilane (61.2 mg, 0.175 mmol) and **ZnP–Bpin** (20.4 mg, 0.0192 mmol) in DME (5 mL) and H_2O (0.1 mL) was deoxygenized by bubbling with nitrogen for 30 min. To this mixture were added dichlorobis(triphenylphosphine)palladium(II) (4.7 mg, 0.00670 mmol) and $Ba(OH)_2 \cdot 8H_2O$ (58.2 mg, 0.184 mmol). The resulting mixture was heated to 80 °C and stirred for 0.5 h at this temperature. After cooling, the resulting mixture was filtered through a pad of silica gel and washed with CH_2Cl_2. After evaporation, the residue was subjected to silica gel column chromatography (hexane/toluene = 4/1 to 2/1, $R_f = 0.18$ (hexane/toluene = 4/1)) followed by preparative

GPC (toluene as an eluent, $t_R = 74$ min) to give 11.2 mg (0.00928 mmol, 48% yield) of **ZnP**–[**Si$_2$**] as purple solids. ^{1}H NMR (C$_6$D$_6$): $\delta = 9.33–9.35$ (m, 6H), 9.21 (d, $J = 4.5$ Hz, 2H), 8.47–8.48 (m, 6H), 8.35 (d, $J = 8.1$ Hz, 2H), 8.04 (t, $J = 1.7$ Hz, 3H), 7.79 (d, $J = 8.1$ Hz, 2H), 7.61–7.64 (m, 2H), 7.27–7.39 (m, 3H), 1.56 (s, 36 H), 1.54 (s, 18H), 0.61 (s, 6H), 0.56 (s, 6H). ^{13}C NMR (C$_6$D$_6$): $\delta = 150.97, 150.91, 150.53, 149.00, 143.99, 143.14, 143.11, 137.79, 134.37, 134.30, 132.56, 132.49, 132.39, 132.28, 130.42, 130.30, 128.95, 128.36, 128.21, 128.00, 127.64, 122.69, 122.65, 121.24, 121.01, 35.31, 32.00, −3.40$. ^{29}Si NMR (C$_6D_6$): $\delta = −21.04, −21.44$. HRMS(FAB): Calc. for C$_{78}$H$_{92}$ON$_4$Si$_2$Zn: 1204.6152. Found: 1204.6177.

4.9. Spectral measurements

Steady-state fluorescence spectra were measured on a spectrofluorophotometer (Shimazu RF-5300 PC). These spectra were taken with about 10^{-6} M solutions. The time-resolved fluorescence spectra were measured by a single photon counting method using a streakscope (Hamamatsu Photonics, C4334-01) equipped with a polychromater and a SHG (400 nm) of a Ti:Sappire laser (Spectra-Physics, Tsunami 3950-L2S, 1.5 ps fwhm) as excitation source. Nanosecond laser flash photolysis experiments were carried out using the 532 nm light from SHG of a Nd:YAG laser (Spectra-Physics, Quanta-Ray GCR-130, 6 ns fwhm) as an excitation source. For the transient absorption spectra in the near-IR region (600–1200 nm), monitoring light from a pulsed Xe-lamp was detected with a Ge-APD detector. For spectra in the visible region (400–1000 nm), a photomultiplier tube or a Si-PIN photodiode was used as a detector. All the samples in a quartz cell (1 cm × 1 cm) were deaerated by bubbling argon gas through the solution.

4.10. X-ray crystallography

Crystallographic data for the structural analysis has been deposited with the Cambridge Crystallographic Data Centre. CCDC No. 299888 for compound *i*-**PrO**–**Si$_4$**(*anti*)–**O*i*-Pr**.

Acknowledgments

Appendix A. Supplementary data

CCDC No. 299888 for compound *i*-**PrO**–**Si$_4$**(*anti*)–**O*i*-Pr**. Copies of this information may be obtained free of charge from: The Director, CCDC, 12 Union Road, Cambridge CB2 1EZ, UK (fax (int. code): +44 1223 336 033 or e-mail: deposit@ccdc.cam.ac.uk or www: www:http://www.ccdc.cam.ac.uk). Supplementary data associated with this article can be found, in the online version, at doi:10.1016/j.jorganchem.2006.05.062.

References

[1] (a) D.M. Guldi, Chem. Soc. Rev. 31 (2002) 22;
(b) H. Imahori, Y. Mori, Y. Matano, J. Photochem. Photobiol. C 4 (2003) 51.
[2] H. Imahori, Y. Sekiguchi, Y. Kashiwagi, T. Sato, Y. Araki, O. Ito, H. Yamada, S. Fukuzumi, Chem. Eur. J. 10 (2004) 3184.
[3] A. Harriman, Angew. Chem., Int. Ed. 43 (2004) 4985.
[4] For recent reviews: (a) M.E. El-Khouly, O. Ito, P.M. Smith, F. D'Souza, J. Photochem. Photobiol. C 5 (2004) 79;
(b) H. Imahori, Org. Biomol. Chem. 2 (2004) 1425.
[5] (a) M.R. Wasielewski, Chem. Rev. 92 (1992) 435;
(b) D. Gust, T.A. Moore, A.L. Moore, Acc. Chem. Res. 26 (1993) 198;
(c) A. Harriman, J.P. Sauvage, Chem. Soc. Rev. 25 (1996) 41;
(d) A. Osuka, N. Mataga, T. Okada, Pure. Appl. Chem. 69 (1997) 797;
(e) D. Gust, T.A. Moore, in: K.M. Kadish, K.M. Smith, R. Guilard (Eds.), The Porphyrin Handbook, vol. 8, Academic Press, San Diego, 2000, p. 153;
(f) D. Gust, T.A. Moore, A.L. Moore, Acc. Chem. Res. 34 (2001) 40;
(g) P.D. Harvey, in: K.M. Kadish, K.M. Smith, R. Guilard (Eds.), The Porphyrin Handbook, vol. 18, Elsevier, Amsterdam, 2003, p. 63;
(h) D. Kim, A. Osuka, Acc. Chem. Res. 37 (2004) 735.
[6] (a) H. Imahori, K. Hagiwara, T. Akiyama, S. Taniguchi, T. Okada, Y. Sakata, Chem. Lett. (1995) 265;
(b) H. Imahori, K. Tamaki, H. Yamada, K. Yamada, Y. Sakata, Y. Nishimura, I. Yamazaki, M. Fujitsuka, O. Ito, Carbon 38 (2000) 1599.
[7] (a) P. Liddel, A.N. Macpherson, J. Sumida, L. Demanche, A.L. Moore, T.A. Moore, D. Gust, Photochem. Photobiol. 59S (1994) 36S;
(b) D. Kuciauskas, S. Kin, G.R. Seely, A.L. Moore, T.A. Moore, D. Gust, T. Drovetskaya, C.A. Reed, P.D.W. Boyd, J. Phys. Chem. 100 (1996) 15926.
[8] (a) H. Imahori, Y. Sakata, Adv. Mater. 9 (1997) 537;
(b) D. Gust, T.A. Moore, A.L. Moore, J. Photochem. Photobiol. B 58 (2000) 63.
[9] H. Imahori, K. Hagiwara, T. Akiyama, M. Aoki, S. Taniguchi, T. Okada, M. Shirakawa, Y. Sakata, Chem. Phys. Lett. 263 (1996) 545.
[10] K. Ohkubo, H. Imahori, J. Shao, Z. Ou, K.M. Kadish, Y. Chen, G. Zheng, R.K. Pandey, M. Fujitsuka, O. Ito, S. Fukuzumi, J. Phys. Chem. A 106 (2002) 10991.
[11] R.A. Marcus, Angew. Chem., Int. Ed. 32 (1993) 1111.
[12] H. Imahori, H. Yamada, D.M. Guldi, Y. Endo, A. Shimomura, S. Kundu, K. Yamada, T. Okada, Y. Sakata, S. Fukuzumi, Angew. Chem., Int. Ed. 41 (2002) 2344.
[13] H. Imahori, K. Hagiwara, M. Aoki, T. Akiyama, S. Taniguchi, T. Okada, M. Shirakawa, Y. Sakata, J. Am. Chem. Soc. 118 (1996) 11771.
[14] H. Imahori, M.E. El-Khouly, M. Fujitsuka, O. Ito, Y. Sakata, S. Hukuzumi, J. Phys. Chem. A 105 (2001) 325.
[15] A.S.D. Sandanayaka, K. Ikeshita, Y. Araki, N. Kihara, Y. Furusho, T. Takata, O. Ito, J. Mater. Chem. 15 (2005) 2276.
[16] H. Imahori, K. Tamaki, Y. Araki, T. Hasobe, O. Ito, A. Shimomura, S. Kundu, T. Okada, Y. Sakata, S. Fukuzumi, J. Phys. Chem. A 106 (2002) 2803.
[17] T.D.M. Bell, T.A. Smith, K.P. Ghiggino, M.G. Ranasinghe, M.J. Shephard, M.N. Paddon-Row, Chem. Phys. Lett. 268 (1997) 223.

[18] (a) K. Yamada, H. Imahori, Y. Nishimura, I. Yamazaki, Y. Sakata, Chem. Lett. (1999) 895;
(b) A. Sato, K. Tashiro, K. Saigo, T. Aida, K. Yamanaka, M. Fujitsuka, O. Ito, in: Proceedings of the 83rd Annual Meeting of the Chemical Society of Japan, Tokyo, March, 2003. Abstract No. 4C8-01;
(c) S.A. Vail, P.J. Krawczuk, D.M. Guldi, A. Palkar, L. Echegoyen, J.P.C. Tomé, M.A. Fazio, D.I. Schuster, Chem. Eur. J. 11 (2005) 3375.

[19] (a) J. Ikemoto, K. Takimiya, Y. Aso, T. Otsubo, M. Fujitsuka, O. Ito, Org. Lett. 4 (2002) 309;
(b) T. Nakamura, M. Fujitsuka, Y. Araki, O. Ito, J. Ikemoto, K. Takimiya, Y. Aso, T. Otsubo, J. Phys. Chem. B 108 (2004) 10700.

[20] Reviews and accounts: (a) M. Kumada, K. Tamao, Adv. Organomet. Chem. 6 (1968) 19;
(b) R.D. Miller, J. Michl, Chem. Rev. 89 (1989) 1359;
(c) R. West, in: E.W. Abel, F.G.A. Stone, G. Wilkinson (Eds.), Comprehensive Organometallic Chemistry II, Pergamon Press, Oxford, 1995, p. 77;
(d) M. Kira, T. Miyazawa, in: Z. Rappoport, Y. Apeloig (Eds.), The Chemistry of Organic Silicon Compounds, vol. 2, Wiley, Chichester, 1998, p. 1311;
(e) J. Michl, R. West, in: R.G. Jones, W. Ando, J. Chojnowski (Eds.), Silicon-Containing Polymers, Kulwer Academic publishers, Dordrecht, 2000, p. 499;
(f) R. West, in: Z. Rappoport, Y. Apeloig (Eds.), The Chemistry of Organic Silicon Compounds, vol. 3, Wiley, Chichester, 2001, p. 541;
(g) H. Tsuji, J. Michl, A. Toshimitsu, K. Tamao, J. Syn. Org. Chem. Jpn. 60 (2002) 762;
(h) H. Tsuji, J. Michl, K. Tamao, J. Organomet. Chem. 685 (2003) 9;
(i) Y. Hatanaka, J. Organomet. Chem. 685 (2003) 207.

[21] (a) K. Tamao, H. Tsuji, M. Terada, M. Asahara, S. Yamaguchi, A. Toshimitsu, Angew. Chem., Int. Ed. 39 (2000) 3287;
(b) H. Tsuji, A. Toshimitsu, K. Tamao, J. Michl, J. Phys. Chem. A 105 (2001) 10246;
(c) H. Tsuji, M. Terada, A. Toshimitsu, K. Tamao, J. Am. Chem. Soc. 125 (2003) 7486;
(d) H. Mallesha, H. Tsuji, K. Tamao, Organometallics 23 (2004) 1639;
(e) H. Tsuji, A. Fukazawa, S. Yamaguchi, A. Toshimitsu, K. Tamao, Organometallics 23 (2004) 3375;
(f) A. Fukazawa, H. Tsuji, K. Tamao, J. Am. Chem. Soc. 128 (2006) 6800.

[22] (a) Some representative works on conformation dependence of the electronic properties of oligosilanes and the conformation control of the silicon chain done by other research groups. B. Albinsson, H. Teramae, J.W. Downing, J. Michl, Chem. Eur. J. 2 (1996) 529;
(b) R. Imhof, H. Teramae, J. Michl, Chem. Phys. Lett. 270 (1997) 500;
(c) K. Obata, C. Kabuto, M. Kira, J. Am. Chem. Soc. 119 (1997) 11345;
(d) S. Mazières, M.K. Raymond, G. Raabe, A. Prodi, J. Michl, J. Am. Chem. Soc. 119 (1997) 6682;
(e) R. Tanaka, M. Unno, H. Matsumoto, Chem. Lett. (1999) 595;
(f) K. Obata, M. Kira, Organometallics 18 (1999) 2216;
(g) I. El-Sayed, Y. Hatanaka, C. Muguruma, S. Shimada, M. Tanaka, N. Koga, M. Mikami, J. Am. Chem. Soc. 121 (1999) 5095;

(h) I. El-Sayed, Y. Hatanaka, S. Onozawa, M. Tanaka, J. Am. Chem. Soc. 123 (2001) 3597.

[23] H. Tsuji, M. Sasaki, Y. Shibano, M. Toganoh, T. Kataoka, Y. Araki, K. Tamao, O. Ito, Bull. Chem. Soc. Jpn. 79 (2006) 1338.

[24] In this paper, X–Si_4–X means that X-groups are attached directly to the terminal silicon atoms, while X–[Si_4]–X means that X-groups are placed on the *para*-position of the benzene rings which are connected to the terminal silicon atoms, e.g., Cl–Si_4–Cl: 1,4-dichlorotetrasilane and Br–[Si_4]–Br: 1,4-bis(4-bromophenyl)tetrasilane.

[25] A. Kawachi, K. Tamao, J. Organomet. Chem. 601 (2000) 259.

[26] M. Miggini, G. Scorrano, M. Prato, J. Am. Chem. Soc. 115 (1993) 9798.

[27] (a) N. Armaroli, G. Marconi, L. Echegoyen, J.-P. Bourgeois, F. Diederich, Chem. Eur. J. 6 (2000) 1629;
(b) V. Chukharev, N.V. Tkachenko, A. Efimov, D.M. Guldi, A. Hirsch, M. Scheloske, H. Lemmetyinen, J. Phys. Chem. B 108 (2004) 16377;
(c) H. Imahori, N.V. Tkachenko, V. Vehmanen, K. Tamaki, H. Lemmetyinen, Y. Sakata, S. Fukuzumi, J. Phys. Chem. A 105 (2001) 1750;
(d) T.D.M. Bell, K.P. Ghiggino, K.A. Jolliffe, M.G. Ranasinghe, S.J. Langford, M.J. Shephard, M.N. Paddon-Row, J. Phys. Chem. A 106 (2002) 10079;
(e) N.V. Tkachenko, H. Lemmetyinen, J. Sonoda, K. Ohkubo, T. Sato, H. Imahori, S. Fukuzumi, J. Phys. Chem. A 107 (2003) 8834.

[28] A. Harriman, G. Porter, N. Sealre, J. Chem. Soc., Faraday Trans. 2 76 (1979) 1515.

[29] H. Tsuji, Y. Shibano, T. Takahashi, M. Kumada, K. Tamao, Bull. Chem. Soc. Jpn. 78 (2005) 1334.

[30] The larger molecular movement of the *syn* isomer even in the solid state has been observed by CSA measurement. H. Tsuji, H. Kaji, K. Tamao, unpublished results.

[31] $\Phi_{FL}^{Dyad}/\Phi_{FL}^{Ref}$ and $\tau_{FL}^{Dyad}/\tau_{FL}^{Ref}$ are described as following equations:

$$\frac{\Phi_{FL}^{Dyad}}{\Phi_{FL}^{Ref}} = \frac{\frac{k_r^{Dyad}}{k_r^{Dyad}+k_{nr}^{Dyad}+k_{EN,ET}^{Dyad}}}{\frac{k_r^{Ref}}{k_r^{Ref}+k_{nr}^{Ref}}}$$

$$\frac{\tau_{FL}^{Dyad}}{\tau_{FL}^{Ref}} = \frac{k_r^{Ref} + k_{nr}^{Ref}}{k_r^{Dyad} + k_{nr}^{Dyad} + k_{EN,ET}^{Dyad}}$$

where k_r, k_{nr} and $k_{EN,ET}$ are the rate constants of radiative relaxation, non-radiative relaxation and EN and ET processes, respectively; superscript indicates the dyads or the reference porphyrin. The $\Phi_{FL}^{Dyad}/\Phi_{FL}^{Ref}$ values are essentially the same as the $\tau_{FL}^{Dyad}/\tau_{FL}^{Ref}$ values if the k_r^{Dyad} and k_{nr}^{Dyad} values are the same as that of the reference porphyrin.

[32] H. Sakurai, K. Tominaga, T. Watanabe, M. Kumada, Tetrahedron Lett. 45 (1966) 5493.

[33] G. Mignani, A. Kramer, G. Pucetti, I. Ledoux, G. Soula, J. Zyss, Mol. Eng. 1 (1991) 11.

[34] A.G. Hyslop, M.A. Kellett, P.M. Iovine, M.J. Therien, J. Am. Chem. Soc. 120 (1998) 12676.

[35] K.E. Ruehl, K. Matyjaszewski, J. Organomet. Chem. 410 (1991) 1.

[36] H. Gilman, S. Inoue, J. Org. Chem. 29 (1964) 3418.